J Mol Model (2013) 19:1407–1415
DOI 10.1007/s00894-012-1692-9

ORIGINAL PAPER

DFT and TDDFT study on the electronic structure and photoelectrochemical properties of dyes derived from cochineal and lac insects as photosensitizer for dye-sensitized solar cells

Wichien Sang-aroon · Seksan Laopha · Phrompak Chaiamornnugool · Sarawut Tontapha · Samarn Saekow · Vittaya Amornkitbamrung

Received: 25 June 2012 / Accepted: 12 November 2012 / Published online: 6 December 2012

Abstract Essential parameters related to the photoelectrochemical properties, such as ground state geometries, electronic structures, oxidation potential and electron driving force, of cochineal insect dyes were investigated by DFT and TDDFT at the B3LYP/6-31+G(d,p) level of the theory. The results show that the major charge flow dynamic for all dyes is the HOMO→LUMO transition. The bi-coordinated binding mode, in which the dye uses one carboxyl- and hydroxyl oxygen bound to Ti(IV), is found for all dye-TiO_2 systems. Additionally, the doubly bi-coordinated binding mode in which the dye used both carboxyl groups bound to two Ti(IV) is also possible due to high energy distribution occupied at anchoring groups. This study highlights that most of these insect dyes can be good photosensitizers in dye-sensitized solar cells based on their strong binding to the TiO_2 surface, good computed excited state oxidation potential and thermodynamically favored electron driving force.

Keywords Lac dye · Natural pigments · Dye-sensitized solar cell · DFT calculation

W. Sang-aroon · P. Chaiamornnugool · S. Tontapha · S. Saekow · V. Amornkitbamrung (✉)
Integrated Nanotechnology Research Center,
Department of Physics, Faculty of Science, Khon Kaen University,
Khon Kaen 40002, Thailand
e-mail: vittaya@kku.ac.th

W. Sang-aroon
e-mail: wichien.sa@rmuti.ac.th

S. Laopha
Materials Science and Nanotechnology Program,
Faculty of Science, Khon Kaen University,
Khon Kaen 40002, Thailand

W. Sang-aroon
Department of Chemistry, Faculty of Engineering,
Rajamangala University of Technology Isan, Khon Kaen Campus,
Khon Kaen 40000, Thailand

V. Amornkitbamrung
Thailand Center of Excellence in Physics, CHE,
Ministry of Education, Bangkok 10400, Thailand

Introduction

Since 1991, the dye-sensitized solar cell (DSSC), often called the "Grätzel cell" [1] has attracted the extensive interest of many researchers from both a fundamental and a practical perspective [2–24] as a low-cost and high efficiency solar electricity system. In DSSC, the dye, as photosensitizer, plays a major role in absorbing sunlight and transporting electrons into the conduction band of the semiconductor, transforming solar energy to electricity. So far, DSSC sensitized by Ru-containing compounds have achieved the highest solar to electricity conversion efficiency (~11 %) [25, 26]. Even though such DSSCs possess high efficiency, disadvantages in this system also exist. The main problem is that the sensitizer used in DSSC are noble metal compounds that are limited in amount causing of high product costs. In addition, toxicity to humans and the environment is found. Thus, non-metallic organic dyes as well as natural dyes have attracted interest in this field due to their cheapness, abundance and environmental friendliness.

Recently, DSSC using some organic dyes as sensitizers have been reported with efficiency as high as 9.8 % [27]. Regarding natural dyes, a group of cyanin

[28–39], carotenoid [40, 41], tannin [42], chlorophyll [43] and coumarin dye and its derivatives [44–46] have been utilized as sensitizers. A promising approach to improve the performance of DSSC is to search for new dyes or structural modification of existing dyes. A natural dye can be extracted from many parts of vegetables, flowers and trees, and some dyes can be extracted from insects. Recent work has reported DSSC performance using dyes extracted from the fungus *Monascus*, with the highest overall conversion efficiency of 2.3 % being reached [47]. Theoretical work has also supported experimental results [48]. Thus, dyes derived from fungi as well as small-scale insects are interesting to test for photosensitization in DSSC. Carminic acid (CA) can be extracted from the body and eggs of the cochineal insect (*Dactylopius coccus*). Lac dye (LA) is a natural reddish dye stuff extracted from stick lac, which is a secretion of the insect *Coccus laccae* (*Laccifer Lacca Kerr*). Both dyes have been used extensively as a natural food additive, cosmetics and, especially, as a colorant for silk and cotton dyeing. The pigments belong to the group of anthraquinones, which are water-soluble and can be extracted with water or alcohols. The main pigment in cochineals is CA while LA contains several pigments (Lac A–E) as shown in Fig. 1. Photosensitization and photocurrent switching in CA/TiO_2 hybrid material has been reported [49]. There is evidence that a CA/TiO_2 system may be a good starting point for the development of photofuel cells [50]. There are several advantages to apply this kind of insect dye as a photosensitizer in DSSC, including its molecular structure, which is composed of several potential anchoring groups (-COOH and -OH) that can bind with TiO_2 surface; stability to a wide range of pH, light and heat; nontoxic to the environment and natural abundance.

According to DSSC performance, the electronic structure of the dye and energy level of the semiconductor have to be matched in order to satisfy the electron transfer process. An understanding of electronic, optical, and redox properties of the dye is necessary. Thus, in this work, the electronic structure, optical properties, oxidation potential and electron injection force relevant to charge transfer of CA and LA were investigated using density functional theory (DFT) and time dependent (TD) DFT.

Computational methods

The ground-state geometries of CA and LA were optimized with DFT method at the B3LYP/6-31+G(d,p) level of theory [51–55]. The free energy change (in eV) for electron injection from dyes to TiO_2 surface can be expressed as [56]:

$$\Delta G^{inject} = E_{OX}^{dye*} - E_{CB}^{TiO_2} \quad (1)$$

where E_{OX}^{dye*} is the oxidation potential of the dyes in the excited state. Based on the Rehm and Weller equation [57], E_{OX}^{dye*} can be estimated by

$$E_{OX}^{dye*} = E_{OX}^{dye} - E_{00} + \omega_r \quad (2)$$

where E_{OX}^{dye} is the oxidation potential of the dyes in the ground state while E_{00} is adiabatic energy difference between excited and ground states and ω_r is a coulombic stabilization term. As noted in a previous work [58], the latter term can be negligible, so E_{OX}^{dye*} is estimated approximately as $E_{OX}^{dye} - E_{00}$. $E_{CB}^{TiO_2}$ corresponds to the conduction band of the TiO_2 semiconductor. The $E_{CB}^{TiO_2} = -4.0\,\text{eV}$ [59] used in this work was obtained from experiment because the presented value was observed under conditions in which the semiconductor is in contact with aqueous redox solution at fixed pH [60]. Recently, Preat et al. [61] proposed an equation to calculate ΔG^{inject} reliably in the relaxed excited state; the ΔG^{inject} calculated by unrelaxed paths differs from that of the relaxed path by approximately 0.5 eV. The latter work concluded that calculation using the unrelaxed path is reliable. Thus, in this work, ΔG^{inject} for the dyes was estimated using the unrelaxed path. Single-point calculations at the same level of theory were employed for solvent-effect computations using the polarizable continuum model (PCM) of Tomasi and coworkers [62–68]. The integral-equation formalism (IEF) PCM [62, 65] was used in single-point calculations for the PCM solvent effect. The molecular cavity models used in the PCM models are UAKS [69]. Electronic transitions were examined by single-point calculations using the ground-state geometries performed at TDDFT/B3LYP/6-31+G(d,p) in vacuo and TDDFT/IEF-PCM(UAKS)/B3LYP/6-31+G(d,p) level in water. To analyze the acidity of the carboxylic and hydroxyl groups of the dyes, deprotonation energies (ΔE_H) for each carboxylic and hydroxyl groups (atomic labeled in Fig. 1) were computed based on the following equation:

$$\Delta E_H = E^+ - E_H \quad (3)$$

where E^+ and E_H represent the total energy of the cationic and neutral forms of the dye molecules. All calculations were performed with the Gaussian 03 program package [69]. The program Molekel was utilized to generate molecular graphics [70].

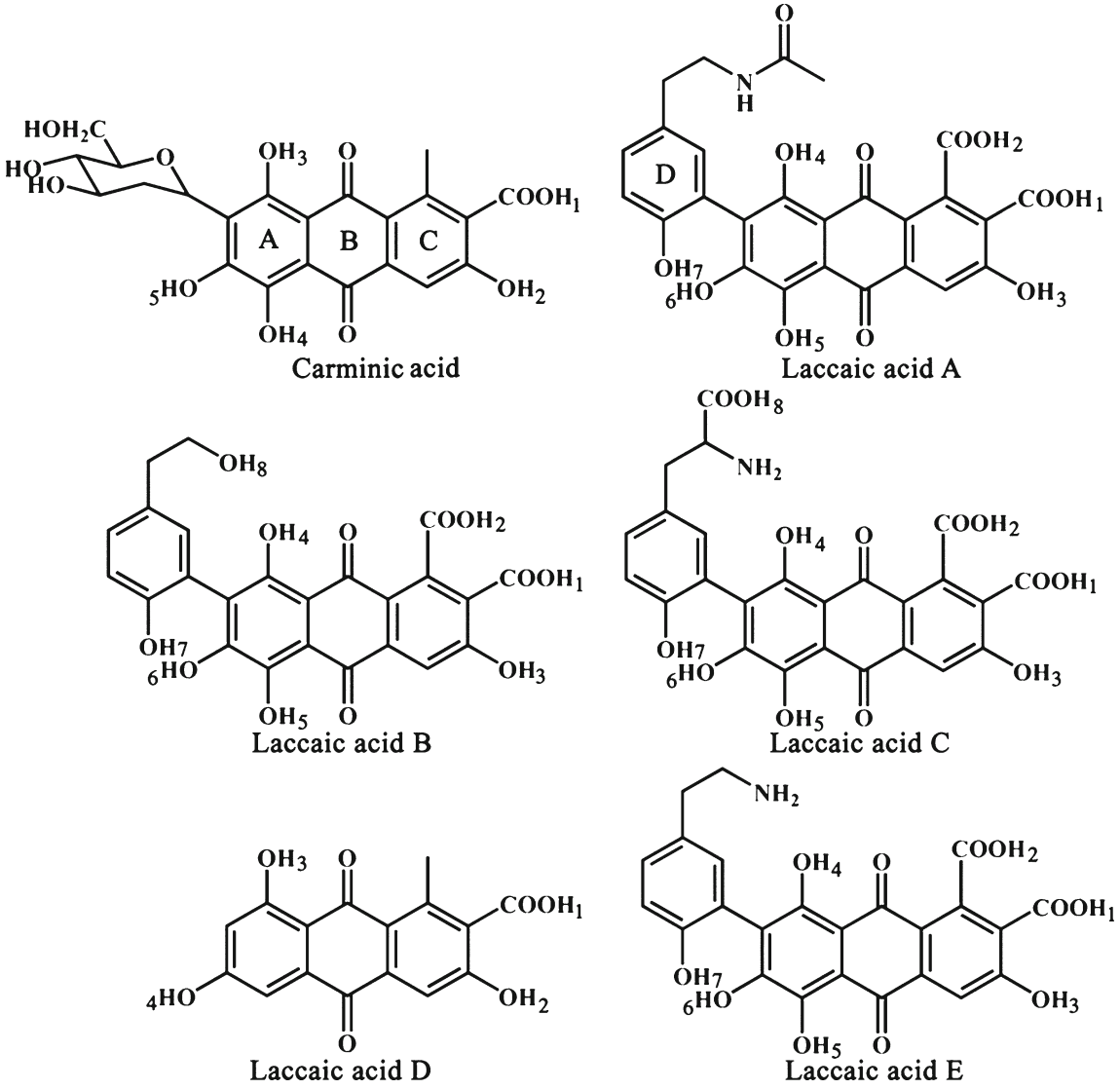

Fig. 1 Chemical structures of carminic acid (CA) and lac dyes (LA)

Results and discussion

Ground state structure and optical properties

The ground state geometries of carminic acid (CA) and all lac dyes (LA) were optimized at B3LYP/6-31+G(d,p) level. The frontier molecular orbital (MO) energies including highest-occupied molecular orbital (HOMO), lowest-unoccupied molecular orbital (LUMO) and energy gap (ΔE_{H-L}) computed in vacuo and water are listed in Table 1. E_{HOMO} of all dyes were more positive (expect for CA) while their E_{LUMO} were more negative going from vacuo to water media. MO energies of CA in this work are close to the previous work based on the same calculation method [71]. As can be seen, differences in the chemical structures of LA_A, B, C and E are their substituents on the phenyl ring D, thus

Table 1 The highest occupied molecular orbital energies (E_{HOMO}), the lowest occupied molecular orbital energies (E_{LUMO}) and energy gap (ΔE_{H-L}) of carminic acid (CA) and all lac dyes (LAs) computed at the B3LYP/6-31+G(d,p) level

Dye	E_{HOMO}[a]		E_{LUMO}[a]		ΔE_{H-L}[a]	
	Vacuo	Water[b]	Vacuo	Water[b]	Vacuo	Water[b]
CA	−6.32	−6.41	−3.04	−3.23	3.28	3.18
LA_A	−6.12	−5.85	−2.91	−3.08	3.21	2.77
LA_B	−6.12	−5.88	−2.91	−3.08	3.21	2.80
LA_C	−6.04	−5.61	−2.83	−2.97	3.21	2.64
LA_D	−6.67	−6.53	−3.07	−3.10	3.60	3.43
LA_E	−6.10	−5.85	−2.88	−2.92	3.22	2.93

[a] In eV

[b] Due to the single-point calculation at IEF-PCM(UAKS)/B3LYP/6-31+G(d,p) level

E_{HOMO} and E_{LUMO} of these four dyes are not much different. A similar result has also been found in their ΔE_{H-L} (in vacuo). LA_D shows lowest E_{HOMO} and E_{LUMO}. Thus, it is noted that phenyl ring D substitution on ring A stabilizes E_{HOMO} and E_{LUMO} of LA_A, B, C and E by their π-conjugate systems leading to lower ΔE_{H-L}. The highest and higher values of ΔE_{H-L} of LA_D and CA may due to sugar moiety substitution and un-substitution, respectively. The ΔE_{H-L} of all dyes are narrower in water media than in vacuo due to the stabilization of their MOs by the polar environment. ΔE_{H-L} of all dyes (in water) are, in decreasing order: LA_D > CA > LA_E > LA_B > LA_A > LA_C.

The UV–vis spectra of all dyes were simulated by single-point calculation using the B3LYP/6-31+G(d,p)-optimized structures computed at TDDFT/B3LYP/6-31+G(d,p) level. The λ_{max} for all dyes, considering as absorption maxima, were obtained from absorption spectra generated from TDDFT computation as shown in Table 2. The results show a ~23–35 nm red shift of λ_{max} from vacuo to water media for all dyes. The computed values are ~13–28 nm lower than the experimental values. The λ_{max} of LA_A is similar to those of crude laccaic acid (containing of LA_A, B and C), in which their λ_{max} were reported to be 490 nm, while absorption maxima at 485 and 493 nm were found for LA_E and CA, respectively [72].

The isovalue plots of five MO (HOMO−2 to LUMO+1) levels for all dyes together with their ΔE_{H-L} are shown in Fig. 2. The HOMO-2 orbitals of all lac dyes (except for LA_D) are localized separately at the phenyl ring A and ring C, especially on the -$COOH_1$ and -OH_3 groups. For, HOMO-1 orbital, more electron distribution is found on the phenyl ring while a much lesser distribution is found on ring C. As can be seen, the phenyl rings D of LA_A, B, C, and E, as well as the sugar ring of CA were perpendicular to the planar core. At

Table 2 Maximum absorption wavelengths (λ_{max}) for UV–vis absorption spectra of CA and all LAs in various media computed at TD/DFT/B3LYP/6-31+G(d,p) level

Dye	Maximum absorption band (nm)		
	Vacuo	H_2O[a]	Exp[b]
CA	442	465	493
LA_A	447	470	490
LA_B	447	470	490
LA_C	445	469	490
LA_D	412	447	–
LA_E	447	472	485

[a] Due to the single-point calculation at IEF-PCM(UAKS)/TDDFT/B3LYP/6-31+G(d,p) level

[b] Taken from [72]

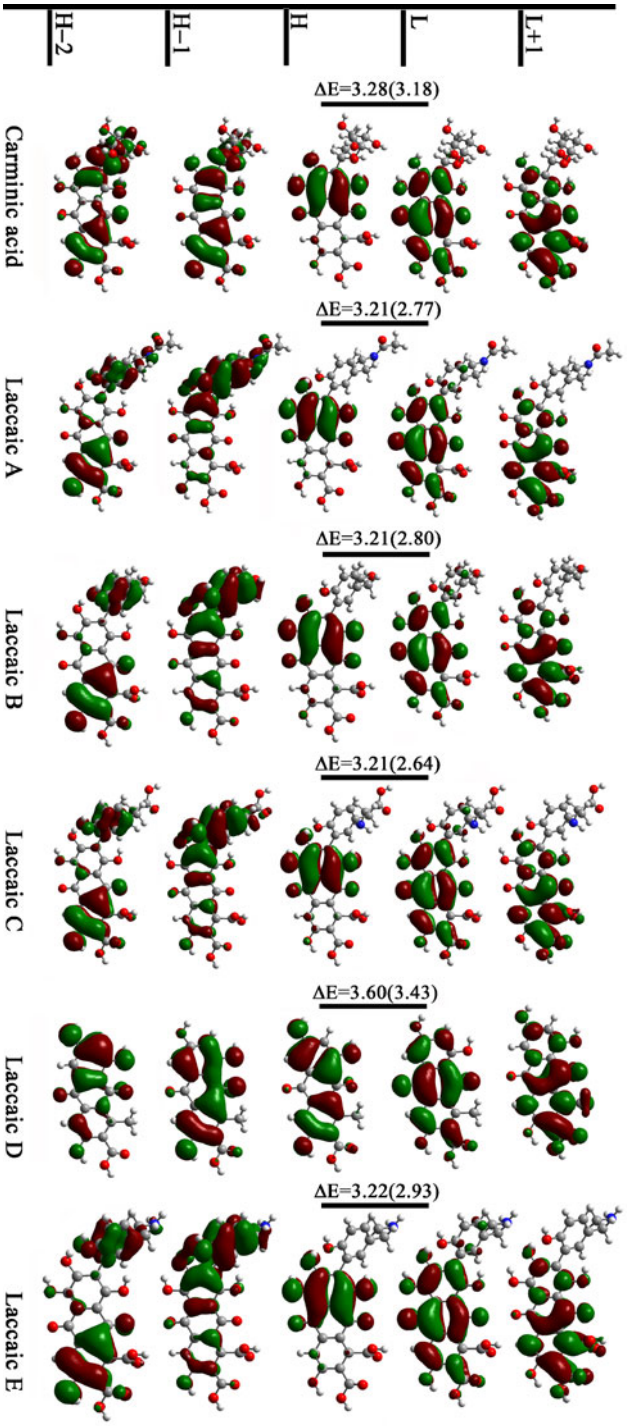

Fig. 2 Isovalue plot of frontier molecular orbital (MO) of CA and LAs and their corresponding energy gap, E_{gap} (eV) in vacuo and in water (*in parenthesis*)

HOMO orbital, energies are contributed mainly on ring A, collapsing to ring B with a conjugated double bond. The energies located mainly on ring B and C of the LUMO are in accordance with the charge movement from the ring A at HOMO. The LUMO+1 of LA_A,

B, C, E is not very different from their LUMO, in which the node of energy is found at $–COOH_2$ as well as $–COOH_1$.

The first three vertical singlet states, major transition characters and oscillating strength of the absorption bands in the UV–vis region for all dyes computed by single-point calculation using TDDFT/B3LYP/6-31+G(d, p) are presented in Table 3. It can be observed that the first transition of all dyes is the HOMO→LUMO found both in water and vacuum environments. HOMO→-LUMO+1 is found as second and third characters for all dyes. HOMO-2→LUMO and HOMO-3→LUMO can be observed in the transitions of all dyes. The HOMO→LUMO+1 can be considered as the possible transition due to its high charge distribution located on both two carboxyl groups with high corresponding oscillating strength and transition character. The possible binding modes of the dye–TiO_2 system are shown in Fig. 3. The bi-coordinated mode formed by the hydroxyl oxygen of $–OH_3$ and carboxyl oxygen of $–COOH_1$ and Ti(IV) (Fig. 3a) were proposed previously for CA [49]. However, for LA_A,B,C,E, the bi-coordinated binding mode may be formed by either $-COOH_1$ or $-COOH_3$ and Ti(IV) due to the nodal charge distribution, which is found on both groups at LUMO+1 orbital. The ability of the anchoring group to chelate with Ti(IV) depends on the deprotonation energy for all –OH and –COOH groups, as tabulated in Table 4. Deprotonation energies (ΔE_H) of the dye were computed from the energy difference between their neutral and cationic forms of various deprotonate sites. The ΔE_H of the first three anchoring groups of LA_A, B, C and E are, in increasing order: $–COOH_1 < –OH_2 < –COOH_3$. These computed parameters confirmed the predicted doubly bi-coordinated mode (Fig. 3b) based on the lower difference in deprotonation energy between $–COOH_3$ and $–COOH_1$ groups (~20 $kcal mol^{-1}$). This kind of binding mode will enhance greater charge transfer from the dye to the TiO_2 surface than another mode in the case of the HOMO→LUMO+1 with more intensive occurrence.

Excited state oxidation potential and electron injection force

Electron transfer from excited state of the dye to conduction band of semiconductor depends on the excited state oxidation potential. E_{OX}^{dye} is estimated as the negative E_{HOMO} based on Koopman's theorem [73]. ΔG^{inject} and E_{OX}^{dye*} are computed from Eqs. 1 and 2, respectively. The computed E_{OX}^{dye}, E_{OX}^{dye*}

Table 3 Vertical singlet states, transition character and oscillating strength (with f>0.01) of absorption bands in UV–vis region of CA and all LAs computed at the TDDFT/B3LYP/6-31+G(d,p) level

Dye	Vacuo			H_2O[a]		
	Energy[b]	Transition character[c]	f	Energy[b]	Transition character[c]	f
CA	2.8041	HOMO→LUMO (85 %)	0.121	2.6626	HOMO→LUMO (87 %)	0.1609
	3.5426	H-2→LUMO (50 %)	0.016	3.5986	H-2→LUMO (42 %)	0.0434
	3.6852	HOMO→L+1 (82 %)	0.070	3.6281	HOMO→L+1 (52 %)	0.2377
LA_A	2.7734	HOMO→LUMO (85 %)	0.166	2.6224	HOMO→LUMO (81 %)	0.2259
	3.5400	HOMO→L+1 (82 %)	0.083	3.3045	H-1→LUMO (92 %)	0.0284
	3.6615	H-3→LUMO (63 %)	0.124	3.4629	HOMO→L+1 (70 %)	0.1264
LA_B	2.7775	HOMO→LUMO (84 %)	0.164	2.6335	HOMO→LUMO (86 %)	0.2366
	2.8564	HOMO→L+1 (83 %)	0.077	2.9900	H-1→LUMO (93 %)	0.0227
	3.0739	H-3→LUMO (61 %)	0.127	3.3950	H-2→LUMO (73 %)	0.1084
LA_C	2.7632	HOMO→LUMO (85 %)	0.162	2.6368	HOMO→LUMO (88 %)	0.2234
	3.5302	HOMO→L+1 (80 %)	0.081	3.4422	H-1→LUMO (84 %)	0.0289
	3.6866	H-3→LUMO (66 %)	0.132	3.5567	H-2→LUMO (45 %)	0.0144
LA_D	3.0088	HOMO→LUMO (72 %)	0.039	2.8023	HOMO→LUMO (80 %)	0.0593
	3.3228	HOMO→L+1 (70 %)	0.027	3.2203	H-1→LUMO (61 %)	0.0213
	3.1825	H-3→LUMO (62 %)	0.468	3.5185	HOMO→LUMO+1 (47 %)	0.1214
LA_E	2.7724	HOMO→LUMO (85 %)	0.164	2.6317	HOMO→LUMO (86 %)	0.2383
	3.5426	H-1→LUMO (40 %)	0.079	2.9509	H-1→LUMO (67 %)	0.0172
	3.0732	HOMO→L+1 (81 %)	0.128	3.3282	HOMO→LUMO+1 (55 %)	0.0336

[a] Due to single-point calculation at IEF-PCM(UAKS)/TDDFT/B3LYP/6-31+G(d,p) level

[b] In eV

[c] Only major contribution to the transitions for each states are in parenthesis

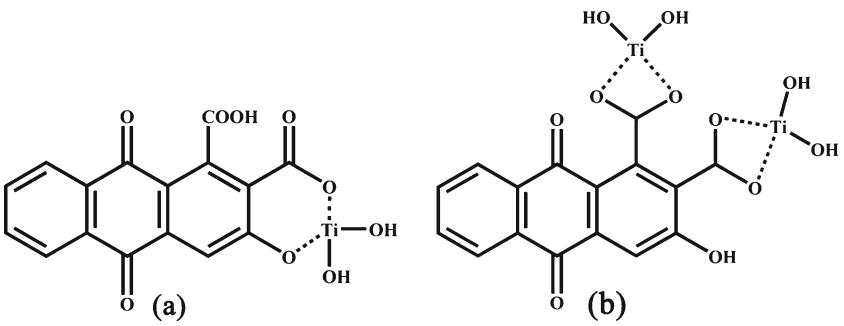

Fig. 3a,b Proposed binding modes of interaction between LA and Ti(IV). **a** Bi-coordinated mode, **b** doubly bi-coordinated mode

and ΔG^{inject} of all dyes in vacuo and water are tabulated in Table 5. LA_D possesses the highest E_{OX}^{dye*} and lowest ΔG^{inject} in both two phases due to the effect of un-substitution on ring A as described above. This means that LA_D is less responsive to the photosensitization and charge transport process in both two phases. On the other hand, the most positive response in photosensitization and dynamic charge flow is LA_C. ΔG^{inject} and E_{OX}^{dye*} computed in water are different from the value computed in vacuo due to the polarization effect on E_{HOMO}. The charge transfer due to photosensitization of all dyes is spontaneous.

Thermodynamically, the spontaneous charge transfer process from the dye excited state to the conduction band of TiO_2 requires LUMO energy with more positive potential than $E_{CB}^{TiO_2}$ (−4.0 eV), while HOMO energy with more negative than redox potential of the I^-/I_3^- electrolyte (±4.80 eV) [74] requires spontaneous charge regeneration. The energy level diagram of the HOMO and LUMO of the dyes and E_{cb} of TiO_2 and redox potential of the electrolyte is depicted in Fig. 4. The LUMOs of all dyes lies over the E_{cb} of TiO_2 while their HOMOs are lower than the reduction potential of electrolyte. Thus, all of them possess a positive response to charge transfer and regeneration related to the photosensitization process.

Relationship between electronic structure of the dyes and photovoltaic performance

The overall efficiency (η) of the DSSC can be calculated from the integral of short-circuit photocurrent density (J_{SC}), open circuit potential (V_{OC}), the fill factor (*ff*) and the intensity of light (I_s), expressed by

$$\eta = \frac{J_{SC} V_{OC} ff}{I_s} \tag{4}$$

From this expression, J_{SC}, V_{OC}, and *ff* are obtained only by experiment. The relationship among these values and electronic structures of the dyes is still not well understood. However, the relationship between V_{OC} and E_{LUMO} of the dyes based on electron injection from LUMO of the dye to E_{cb} of TiO_2 can be expressed as [75]:

$$eV_{OC} = E_{LUMO} - E_{cb} \tag{5}$$

$$V_{OC} = \frac{E_{LUMO} - E_{CB}}{e} \tag{6}$$

According to this expression, the higher the E_{LUMO}, the larger the V_{OC} found. The approximated V_{OC} values based on Eq. 6 for the dyes are tabulated in Table 6. The trend of the V_{OC} of the dyes was found to be similar to E_{OX}^{dye*} and ΔG^{inject}. As mentioned in a previous work [49], where CA–TiO_2 was found to be a good photovoltaic system, all LAs (except for LA_D) will give higher overall efficiency than CA without consideration of any other factors. LA_C and LA_D are found to be the best and the worst sensitizers, respectively, while LA_E, A and B are also expected to show good overall efficiency of their DSSCs.

Table 4 Deprotonation energies[a] (in kcal mol^{-1}) of various anchoring groups of CA and all LAs

Dyes	ΔEH_1	ΔEH_2	ΔEH_3	ΔEH_4	ΔEH_5	ΔEH_6	ΔEH_7	ΔEH_8
CA	342.12	371.22	355.10	360.72	–	–	–	–
LA_A	346.14	368.71	352.16	347.71	356.02	337.01	328.52	
LA_B	347.30	367.85	353.22	348.43	355.74	334.48	328.70	376.96
LA_C	347.98	371.47	353.91	350.05	356.78	337.72	330.13	353.47
LA_D	343.98	352.24	348.08	346.66	–	–	–	–
LA_E	344.47	369.22	352.24	349.18	356.26	335.99	331.03	

[a]Computed using Eq. 7

Table 5 The computed ΔG^{inject}, E_{OX}^{dye*} and E_{OX}^{dye} (all in e*V*) for of CA and all LAs

Dye	Vacuo			H_2O		
	E_{OX}^{dye}	E_{OX}^{dye*}	ΔG^{inject}	E_{OX}^{dye}	E_{OX}^{dye*}	ΔG^{inject}
CA	6.32	3.52	−0.48	6.41	3.75	−0.25
LA_A	6.12	3.35	−0.65	5.85	3.23	−0.77
LA_B	6.12	3.34	−0.66	5.88	3.25	−0.75
LA_C	6.04	3.28	−0.72	5.61	2.97	−1.03
LA_D	6.67	3.66	−0.34	6.53	3.73	−0.27
LA_E	6.10	3.33	−0.67	5.85	3.22	−0.78

Table 6 Estimated open-circuit voltage (V_{OC}) and light harvesting efficiency (LHE) of CA and all LAs

Dye	V_{OC}		LHE	
	Vacuo	Water	Vacuo	Water
CA	0.96	0.77	0.3145	0.3096
LA_A	1.09	0.92	0.3177	0.4056
LA_B	1.09	0.92	0.3145	0.4200
LA_C	1.17	1.03	0.3129	0.4072
LA_D	0.93	0.90	0.0858	0.1276
LA_E	1.12	1.08	0.3145	0.4223

One factor relates to efficiency of DSSC is the performance of the dyes in response to incident light. Based on the light harvesting efficiency (LHE) of the dyes, this value has to be as high as possible to maximize the photocurrent response. The LHE can be expressed as [76]

$$\text{LHE} = 1 - 10^{-\text{A}} = 1 - 10^{-\text{f}} \tag{7}$$

where *A* (*f*) is the absorption (oscillating strength) of the dyes associated to the absorption energy (E_{00}). The computed LHEs for all dyes are shown in Table 6. Based on the result, LA_D is the worst responder to incident light among these dyes. Finally, it can be concluded that all the dyes have HOMO−LUMO energy levels matching the E_{CB} level of TiO_2 and the reduction potential of the electrolyte but LA_C, A, and B are suggested as photosensitizers according to their good computed E_{OX}^{dye*}, ΔG^{inject} and V_{OC} values in which these parameters are believed to relate to overall efficiency of DSSC.

Conclusions

The ground state geometries, electronic structures, and photoelectrochemical redox properties of carminic acid and five lac dyes were evaluated using DFT and TDDFT calculations. The results show that the major electronic transition of all dyes is HOMO→LUMO, while HOMO→LUMO+1 is expected to be the minor transition. All the dyes show favored electron injection (negative ΔG_{inject}) from their excited states to the conduction band edge of TiO_2. The E_{OX}^{dye}, E_{OX}^{dye*} as well as ΔG^{inject} of these lac dyes are quite similar except for LA_D. The calculation result suggests that, based on their good computed redox properties, most lac dyes can be used as efficient photosensitizers in DSSC. In addition, they also show a strong interaction with TiO_2, possible via doubly bi-coordinated mode bound to Ti(IV). Their stabilities to thermal degradation and pH are advantage that make this kind of natural dye promising for use as photosensitizers in DSSC.

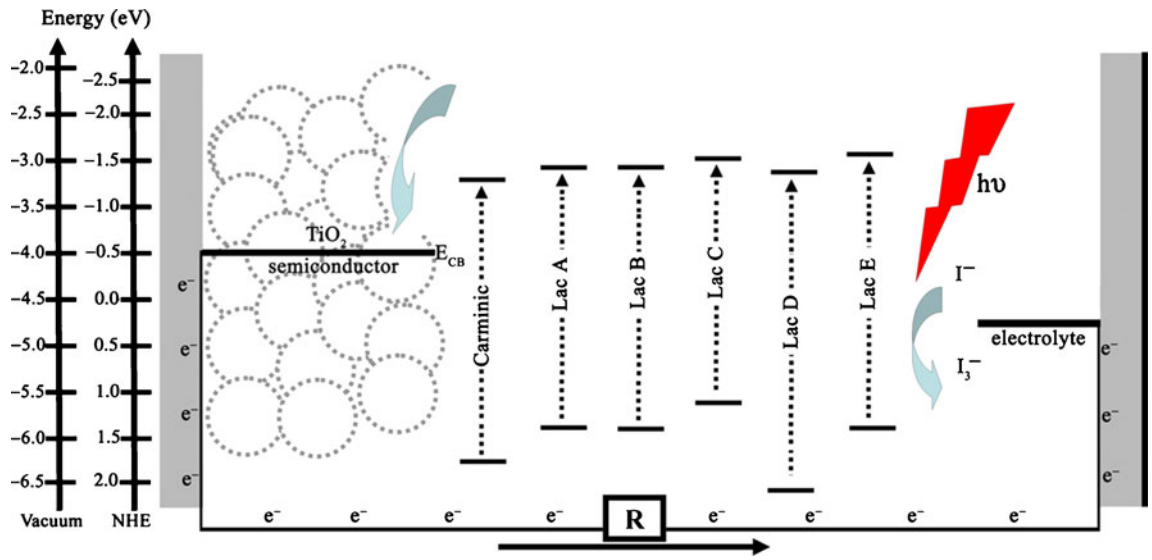

Fig. 4 Schematic energy diagram of CA and LAs, TiO_2 and electrolyte $\left(I^-/I_3^-\right)$. E_{HOMO} and E_{LUMO} of the dyes are in water environment

Acknowledgments This work was supported financially by the National Research University Project, Khon Kaen University through the research grant no. PD.54401. Faculty of Engineering, Khon Kaen Campus and Institute of Research and Development, Rajamangala University of Technology Isan is also acknowledged for partial financial support.

References

1. Ragan BO, Grätzel M (1991) Nature 353:737–740
2. Nazeeruddin MK, Kay A, Rodicio I, Humphry-Baker R, Müller E, Liska P, Vlachopoulos N, Grätzel M (1993) J Am Chem Soc 115:6382–6390
3. Nazeeruddin MK, Péchy P, Renouard T, Zakeeruddin SM, Humphry-Baker R, Comte P, Liska P, Cevey L, Costa E, Shklover V, Spiccia L, Deacon GB, Bignozzi CA, Grätzel M (2001) J Am Chem Soc 123:1613–1624
4. Grätzel M (2004) J Photochem Photobiol A 164:3–14
5. Wang P, Zakeeruddin SM, Moser JE, Nazeeruddin MK, Sekiguchi T, Grätzel M (2003) Nat Mater 2:402–407
6. Hara K, Sato T, Katoh R, Furube A, Ohga Y, Shinpo A, Suga S, Sayama K, Sugihara H, Arakawa H (2003) J Phys Chem B 107:597–606
7. Hara K, Miyamoto K, Abe Y, Yanagida M (2005) J Phys Chem B Lett 109:23776–23778
8. Horiuchi T, Miura H, Uchida S (2004) J Photochem Photobiol A 164:29–32
9. Horiuchi T, Miura H, Sumioka K, Uchida S (2004) J Am Chem Soc 126:12218–12219
10. Kitamura T, Ikeda M, Shigaki K, Inoue T, Anderson NA, Ai X, Lian T, Yanagida S (2004) Chem Mater 16:1806–1812
11. Kim S, Lee JK, Kang SO, Ko J, Yum J-H, Fantacci S, De Angelis F, Censo DD, Nazeeruddin MK, Grätzel M (2006) J Am Chem Soc 128:16701–16707
12. Koumura N, Wang Z-S, Mori S, Miyashita M, Suzuki E, Hara K (2006) J Am Chem Soc 128:14256–14257
13. Wang Z-S, Koumura N, Cui Y, Takahashi M, Sekiguchi H, Mori A, Kubo T, Furube A, Hara K (2008) Chem Mater 20:3993–4003
14. Wang Z-S, Koumura N, Cui Y, Miyashita M, Mori S, Hara K (2009) Chem Mater 21:2810–2816
15. Koumura N, Wang Z-S, Miyashita M, Uemura Y, Sekiguchi H, Cui Y, Mori A, Mori S, Hara K (2009) J Mater Chem 19:4829–4836
16. Zhang X-H, Li C, Wang W-B, Cheng X-X, Wang X-S, Zhang B-W (2007) J Mater Chem 17:642–649
17. Zhang X-H, Wang Z-S, Cui Y, Koumura N, Furube A, Hara K (2009) J Phys Chem C 113:13409–13415
18. Hagberg DP, Edvinsson T, Marinado T, Boschloo G, Hagfeldt A, Sun L-C (2006) Chem Commun 2245-2247
19. Hagberg DP, Yun J-H, Lee JK, Angelis FD, Marinado T, Karlsson KM, Humphry-Baker R, Sun L-C, Hagfeldt A, Grätzel M, Nazeeruddin MK (2008) J Am Chem Soc 130:6259–6266
20. Ning Z, Zhang Q, Wu WJ, Pei HC, Liu B, Tian H (2008) J Org Chem 73:3791–3797
21. Ning Z, Zhang Q, Pei HC, Luan JF, Lu CG, Cui YP, Tian H (2009) J Phys Chem C 113:10307–10313
22. Liu B, Zhu W, Zhang Q, Wu W, Xu M, Ning Z, Xie Y, Tian H (2009) Chem Commun 1766-1768
23. Zhang GL, Bala H, Cheng YM, Shi D, Lv XJ, Yu QJ, Wang P (2009) Chem Commun 2198-2200
24. Zeng WD, Cao YM, Bai Y, Wang YH, Shi YS, Zhang M, Wang FF, Pan CY, Wang P (2010) Chem Mater 22:1915–1925
25. Chiba Y, Islam A, Watanabe Y, Komiya R, Koide N, Han LY (2006) Jpn J Appl Phys 45:638–642
26. Buscaino R, Baiocchi C, Barolo C, Medana C, Grätzel M, Nazeeruddin MK, Viscardi G (2008) Inorg Chim Acta 361:798–805
27. Sirimanne PM, Senevirathna MKI, Premalal EVA, Pitigala PKDDP, Sivakumar V, Tennakone K (2006) J Photochem Photobiol A 177:324–327
28. Hao S, Wu J, Huang Y, Lin J (2006) Sol Energy 80:209–214
29. Polo AS, Murakami Iha NY (2006) Sol Energ Mat Sol Cell 90:1936–1944
30. Wongcharee K, Meeyoo V, Chavadej S (2007) Sol Energ Mat Sol C 91:566–571
31. Zhang D, Lanier SM, Downing JA, Avent JL, Lumc J, McHale JL (2008) J Photochem Photobiol A 195:72–80
32. Roy MS, Balraju P, Kumar M, Sharma GD (2008) Sol Energ Mat Sol C 92:909–913
33. Fernando JMRC, Senadeera GKR (2008) Curr Sci 95:663–666
34. Calogero G, Marco GD (2008) Sol Energ Mat Sol C 92:1341–1346
35. Dai Q, Rabani J (2002) J Photochem Photobiol A 148:17–24
36. Cherepy NJ, Smestad GP, Grätzel M, Zhang JZ (1997) J Phys Chem B 101:9342–9351
37. Luo P, Niu H, Zheng G, Bai X, Zhang M, Wang W (2009) Spectrochim Acta Part A 74:936–942
38. Furukawa S, Iino H, Iwamoto T, Kukita K, Yamauchi S (2009) Thin Solid Films 518:526–529
39. Gómez-Ortíz NM, Vázquez-Maldonado IA, Pérez-Espadas AR, Mena-Rejón GJ, Azamar-Barrios JA, Oskam G (2010) Sol Energ Mat Sol C 94:40–44
40. Yamazaki E, Murayama M, Nishikawa N, Hashimoto N, Shoyama M, Kurita O (2007) Sol Energy 81:512–516
41. Espinosa R, Zumeta I, Santana JL, Martínez-Luzardo F, Gonzalez B, Docteur S, Vigil E, Vigil TE (2005) Sol Energ Mat Sol C 85:359–369
42. Kumara GRA, Kaneko S, Okuya M, Onwona-Agyeman B, Konno A, Tennakone K (2006) Energ Mat Sol C 90:1220–1226
43. Wang Z-S, Hara K, Dan-oh Y, Kasada C, Shinpo A, Suga S, Arakawa H, Sugihara H (2005) J Phys Chem B 109:3907–3914
44. Wang Z-S, Cui Y, Hara K, Dan-oh Y, Kasada C, Shinpo A (2007) Adv Mater 19:1138–1141
45. Wang Z-S, Cui Y, Dan-oh Y, Kasada C, Shinpo A, Hara K (2007) J Phys Chem C 111:7224–7230
46. Wang Z-S, Cui Y, Dan-oh Y, Kasada C, Shinpo A, Hara K (2008) J Phys Chem C 112:17011–17017
47. Ito S, Saitou T, Imahori H, Uehara H, Hasegawa N (2010) Energy Environ Sci 3:905–909
48. Sang-aroon W, Saekow S, Amornkitbamrung V (2012) J Photochem Photobiol A 136:35–40
49. Gaweda S, Stochel G, Szacilowski K (2008) J Phys Chem C 112:19131–19141
50. Cracknell JA, Vincent KA, Armstrong FA (2008) Chem Rev 108:2439–2461
51. Parr RG, Young W (1989) Density functional theory of atoms and molecules. Oxford University Press, Oxford
52. Hohenberg P, Kohn W (1964) Phys Rev B 136:864–871
53. Khon W, Sham L (1965) J Phys Rev A 140:1133–1138
54. Beck ADJ (1993) J Chem Phys 98:5648–5652
55. Lee C, Yang W, Parr R (1988) Phys Rev B 37:785–789
56. Katoh R, Furube A, Yoshihara T, Hara K, Fujihashi G, Takano S, Murata S, Arakawa H, Tachiya M (2004) J Phys Chem B 108:4818–4822
57. Rehm D, Weller A (1970) Israel J Chem 8:259–271
58. Goodman JL, Peters KS (1986) J Am Chem Soc 108:1700–1701
59. Asbery JB, Wang YQ, Hao E, Ghosh H, Lian T (2001) Res Chem Intermed 27:393–406
60. Hagfeldt A, Gräetzel M (1995) Chem Rev 95:49–63
61. Preat J, Michaux C, Jacquemin D, Perpète EA (2009) J Phys C 113:16821–16833

62. Tomasi J, Mennucci B, Cancès ET (1999) J Mol Struct (THEOCHEM) 464:211–226
63. Cancès ET, Mennucci B, Tomasi J (1997) J Chem Phys 107:3032–3041
64. Mennucci B, Tomasi J (1997) J Chem Phys 106:5151–5158
65. Mennucci B, Cancès ET, Tomasi J (1997) J Phys Chem B 101:10506–10507
66. Cossi M, Barone V (1998) J Chem Phys 109:6246–6254
67. Barone V, Cossi M, Tomasi J (1997) J Chem Phys 107:3210–3221
68. Cossi M, Scalmani G, Rega N, Barone V (2002) J Chem Phys 117:43–54
69. Frisch MJ et al (2003) Gaussian 03. Revision B.03. Gaussian, Pittsburgh
70. Flükiger P, Lüthi HP, Portmann S, Weber J (2000) MOLEKEL 4.3, Swiss Center for Scientific Computing, Manno (Switzerland)
71. Heera TR, Cindrella L (2010) J Mol Model 16:523–533
72. Balakina GG, Vasiliev VG, Karpova EV, Mamatyuk VI (2006) Dyes Pigments 71:54–60
73. Pearson RG (1998) Inorg Chem 27:734–740
74. Szostek B, Orska-Gawrys J, Surowiee I, Trojanowicz M (2003) J Chromatogr A 1012:179–192
75. Zhang C-R, Liu Z-J, Chen Y-H, Chen H-S, Wu Y-Z, Feng W, Wang D-B (2010) Curr Appl Phys 10:77–83
76. Irfan A, Al-Sehemi AG (2012) J Mol Model 18:4893–4900